Photocatalysis of the Oxygen Reduction Reaction at Adsorbate-Covered Silver

ARTICLE *in* THE JOURNAL OF PHYSICAL CHEMISTRY C · JANUARY 2008

Impact Factor: 4.77 · DOI: 10.1021/jp075143n

6 AUTHORS, INCLUDING:

John McMahon
Fordham University
16 PUBLICATIONS **83** CITATIONS

Photocatalysis of the Oxygen Reduction Reaction at Adsorbate-Covered Silver

John J. McMahon,* Michael Barry, Kristin J. Breen, Anna K. Radziwon, Leanne D. Brooks, and Michael R. Blair

Department of Chemistry, Fordham University, Bronx, New York 10458

Received: July 2, 2007; In Final Form: October 19, 2007

The oxygen reduction reaction, the slow kinetics of which is well-known to limit efficient energy production from fuel cells, is shown to be catalyzed at adsorbate-covered silver electrodes when the electrode is irradiated with wavelengths in the visible and near-ultraviolet. We report the photocurrent dependence on adsorbate molecule, electrode voltage, excitation wavelength, and oxygen content of the solution. Comparison of the photocurrent excitation profile with the modulated electroreflectance spectrum identifies coupling of two resonances to the catalysis; the silver surface plasmon near 400 nm and another resonance near 550 nm assigned to metal-to-adsorbate charge transfer.

Introduction

The slow kinetics of the oxygen reduction reaction (ORR) constitutes the primary hindrance to efficient energy production from fuel cells. Even at Pt, recognized as the best catalyst for the ORR, significant oxygen reduction current is only realized at large overvoltages negative of the thermodynamic equilibrium cell voltage of +1.23 V. Because the output power of a fuel cell is defined by the product of the cell potential (*V*) and current (*I*), , $P = VI$, a drop in the potential lowers the power output and the cell efficiency linearly. Typically, a platinum-catalyzed hydrogen fuel cell operates at moderate current levels at cell voltages close to +0.75 V. This amounts to an overvoltage of −0.48 V below the thermodynamic voltage, thus limiting the efficiency to near 60%. Experiments probing alternatives to platinum catalysis of the electroreduction of oxygen or dispersion methods that limit the costly Pt-loading of catalysts continue to define a vigorous area of research.[1−8]

As discussed by Henglein,[9] photoemission of electrons from finely dispersed silver (either roughened silver electrodes or nanometer-size colloids) can serve to catalyze reduction of solution-bound molecules or even the solvent itself especially in the presence of adsorbed nucleophiles. Catalyzed reduction is facilitated by the lower density of electronic states at the nanometer-size metal structure which slows the rate of electron−hole recombination relative to the speed of the excited electron toward the surface of the metal particle and out into solution. For example, Henglein calculates a 10^{-12} sec electron−hole pair thermalization time at adsorbate-free 3-nm silver particles, which is longer than the 10^{-15} sec diffusion time needed for the photoelectron to travel to the metal surface and to emit into solution where it can be scavenged by available reductants. Adsorbed nucleophiles, like CN^-, I^-, and SH^-, dump excess electrons into the metal further facilitating electron donation to a reductant upon illumination of the metal. Studies at silver electrodes have shown that hydrated electrons, photoemitted from an irradiated electrode surface, can be scavenged by available reductants like protons,[10] carbon dioxide,[11−14] nitrate,[11,13,15] and nitrite,[15] initiating catalysis of the electroreduction of those reductants.

The decay of surface plasmon excitation into single electrons is cited as the source of photoemission by correlation between surface plasmon excitation wavelength and the wavelength of maximum photocurrent. Threshold wavelengths for photoemission currents are lengthened by the roughening of electrode surfaces[12] and by adsorption of polar molecules,[9,16] in much the same way that surface Raman intensity is enhanced at silver at wavelengths longer than that of the surface plasmon.

As in the long-running debate over the SERS enhancement mechanism, long wavelength metal-to-adsorbate charge-transfer excitations, particularly those occurring at surface roughness features, can similarly be expected to contribute to photoemission currents. Resonant coupling between the energy of incident radiation and the energy difference between the filled metal and empty adsorbate electronic states promotes enhancement of the Raman scattered light intensity. It is well understood that the electronic states of the metal and the adsorbate, that are coupled in this photon-driven charge transfer, can be delocalized by mixing with electronic states of nearby metal atoms in the conduction band system of the metal, rendering both resonant enhancement and fluorescence[17] negligible. However, at atomic scale roughness features such as adatom or adcluster surface sites, and congruent with the electronic effects at the nanometer size silver colloids discussed by Henglein,[9] the lower density of states promotes the localization of the charge-transfer excitation and facilitates resonance Raman intensification. By analogy to this surface Raman enhancement mechanism, photon-driven excitation of an electron from a metal adatom surface site to an adsorbate at that site can be expected to yield a radical anion adsorbate that is long-lived because of the absence of a decay mechanism through the conduction band system of the metal substrate. This extension of the lifetime of radical anion adsorbate at adatom roughness sites assures the availability of electrons for reductants arriving at those surface sites.

It is the purpose of this manuscript to report the extension of the photocatalytic studies at silver to include the photocatalysis of the electroreduction of dissolved oxygen. Our interest in the applicability of the photocatalytic method to the oxygen reduction problem was spurred by observations of oxygen involvement in the photochemistry of trans-4-stilbazole adsorbed at a silver electrode.[18]

* Author to whom correspondence should be addressed. Email: mcmahon@fordham.edu. Tel: (718)817-4495. Fax: (718)817-4432.

10.1021/jp075143n CCC: $40.75
Published on Web 01/09/2008

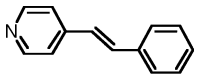

trans-4-stilbazole

The photoproduct, identified as 4′-hydroxy-trans-4-stilbazole, accompanied reduction of dissolved oxygen at the irradiated electrode surface with photochemistry limited to surface active sites identified as Ag^+ sites. Positively charged sites are expected at adatoms or small adclusters of silver.

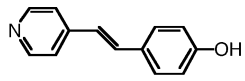

4′-hydroxy-trans-4-stilbazole

While the irreversible photochemistry renders stilbazole-covered silver ineffective at continuous catalysis of oxygen reduction these observations nonetheless prompted a search for an adsorbate, similar to stilbazole, that might be catalytically effective. Realizing that catalysis of oxygen reduction demands study at applied potentials significantly anodic of the voltages needed for catalysis of the previously studied reductants listed above, we sought an adsorbate that was not easily oxidizable. We began our study with the adsorbate bis-1,2-(4-pyridyl)-acetylene (BPA). While retaining nucleophilic nitrogens for complexaion to silver the triple bond bridge provides a less oxidizable adsorbate than double-bonded stilbazole and absence of a ϕ-H bond at the 4′ position leaves BPA photostable relative to stilbazole.

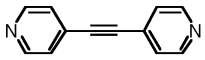

1,2-bis-(4-pyridyl)-acetylene or BPA

We will demonstrate that the oxygen reduction reaction is catalyzed at a BPA-covered silver electrode surface upon irradiation of the surface with light of wavelengths within the visible and near-ultraviolet. Analogous photocatalytic behavior is also reported for I_2-covered silver.

Experimental Methods

Electrochemical measurements were performed in a cell constructed to afford irradiation of the working electrode through a quartz optical flat. The working electrode was a 5.0 mm diameter silver disk mounted in a Teflon cylinder (Pine Instrument Co., Raleigh, NC). The reference electrode was a "no-leak" Ag/AgCl electrode (Cypress Systems, Chelmsford, MA), and electrode potentials are reported relative either to the Ag/AgCl reference or to reversible hydrogen electrode in the actual solution used (RHE). The counter electrode was a platinum wire. Potential control and photocurrent measurements were accomplished with a model 263A potentiostat/galvanostat (Princeton Applied Research, Oak Ridge, TN) interfaced to a microcomputer.

Irradiation of the surface was carried out with either a Spectra Physics 2020−05 argon ion laser or with a 200−500 W Oriel xenon arc source dispersed (20 nm fwhm resolution) through an Oriel model 77250 single monochromator (Newport Corporation, Irvine, CA). The light was focused so as to cover the full surface of the silver electrode as much as possible with the irradiated surface area estimated near 0.150 cm^2 of the available 0.196 cm^2 electrode cross section. Light intensity was measured with a calibrated model 362 power energy meter (Scientech, Boulder, CO) and the photocurrents observed with the xenon arc source were normalized to equal intensity over the wavelength range (650−350 nm). The angle of incidence was 60° to the surface normal. Photocurrent measurements were typically recorded during a 4-second irradiation period afforded by a computer-controlled model LSGZM2 shutter (Vincent Associates, Rochester, NY).

The modulated electroreflectance spectrum of the [bis-1,2-(4-pyridyl)ethylene]-covered silver electrode was recorded with a Cary 219 spectrophotometer (Varian, Inc., Palo Alto, CA). Electrode voltage was modulated by ±0.3 V sinusoidally about a bias voltage of −0.4, −0.5, or −0.6 V at a frequency of 0.1 Hz and averaged over 10 cycles. The component of the electroreflectance that tracked in-phase with the voltage modulated was extracted by Fourier analysis and reported.

Preparation of the silver electrode for photocurrent measurements began with wet polishing with progressively finer (down to 0.05 μm) aluminum oxide powders applied to a felt polishing pad (Buehler Ltd., Lake Bluff, IL). The electrode was rinsed with distilled water and placed in the electrochemical cell with a supporting electrolyte of 3.3 M potassium chloride with the pH adjusted to 1.5 by addition of hydrochloric acid. The electrode was polarized to −1.9 V versus Ag/AgCl for 1 h to effect electrochemical cleaning by hydrogen evolution in the acidic electrolyte. Hydrogen reduction currents were observed to increase and attain a steady-state maximum within the 1-h cleaning period. The applied voltage was then adjusted to −0.3 V and the electrode was subjected to three double potential step oxidation−reduction cycles between −0.3 and +0.2 V with the development of 10 mC anodic charge (50 mC per cm^2 electrode area) per cycle. Extensive roughening of the silver island type was confirmed by atomic force microscopy to accompany this oxidation−reduction cycling procedure. Following electrochemical roughening, the silver was removed from the electrochemical cell and dipped in aqueous solutions that had been saturated with the intended adsorbate, iodine [I_2] or 1,2-bis-(4-pyridyl)-acetylene [BPA]. Large photocurrent signals were observed for iodine dipping periods of 10 min, while overnight dipping improved the photocurrents observed at BPA-covered silver. After dipping, the silver electrode was rinsed with distilled water and returned to the electrochemical cell whose electrolyte had been changed to an aqueous solution of either 0.1 M NaCl or 0.1 M $NaClO_4$ solution and the pH was adjusted to 3.0 by the addition of HCl or $HClO_4$, respectively. Negligible photocurrents were observed when the dipping or electrochemical preroughening steps were avoided. Dipping silver in aqueous saturated iodine solution was shown electrochemically to have generated silver iodide (AgI) at the electrode surface by the coupling of silver oxidation and iodine reduction in the dip. Recognizing this, we alternatively prepared a silver surface that was very photoactive toward reduction of dissolved oxygen by oxidizing polished silver in 0.1 M aqueous potassium iodide but *without* subsequent reduction of the silver iodide film prior to photocurrent measurement in the 0.1 M $NaClO_4$.

The oxygen content of solution was measured with a model sensIon6 dissolved oxygen meter (Hach Co., Loveland, CO). The oxygen content was varied between 0% and 330% air saturation (0−30.29 mg/L) by bubbling either purified oxygen or nitrogen gas. Nitrogen was purified of trace oxygen by passing the gas over heated (600 °C) copper turnings.

1,2-Bis-(4-pyridyl)-ethylene [BPE] (Sigma-Aldrich) was recrystallized from hot water before use in electroreflectance measurements or in the synthesis of BPA. BPA was synthesized as outlined in the doctoral thesis of Tanner,[19] where BPE was

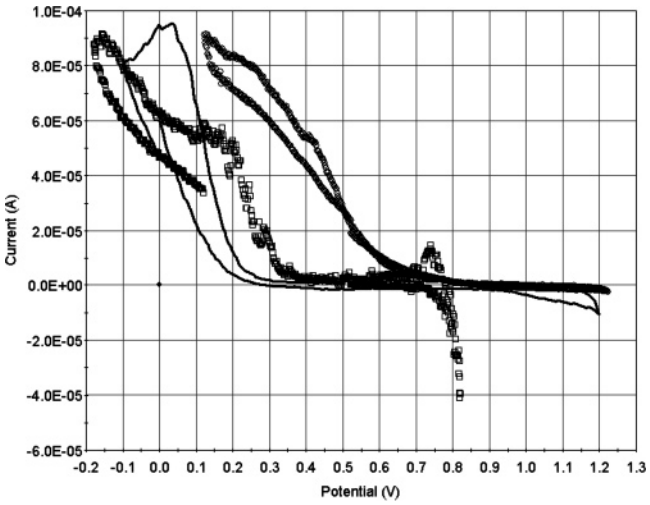

Figure 1. Electroreduction of oxygen at polished gold (—), silver (□), and platinum (○) in aqueous 0.01 M $HClO_4$. Potentials are referenced to the RHE.

first dissolved in 48% HBr. Then, 1 equiv of bromine (Br_2) was added slowly with formation of an orange precipitate. The reaction mixture was refluxed for 1 h. The orange precipitate was collected and treated with 0.2 M NaOH until it turned white. The white precipitate, suspended in a small amount of *tert*-butyl alcohol, was then added to a boiling mixture of *tert*-butyl alcohol and potassium butoxide. This reaction mixture was again refluxed for 1 h. The solvent was removed by evaporation and BPA was extracted from the remaining solid with diethyl ether. With evaporation of the ether solvent BPA crystals were gathered and recrystallized from hot water.

Results and Discussion

Oxygen reduction commences at varied overvoltages dependent upon the cathode material, as demonstrated in Figure 1, where platinum is shown to be a better catalyst for the reaction than either silver or gold. Additionally, silver is limited in its applicability to fuel cell applications in that, unlike platinum or gold, silver oxidizes at potentials well cathodic of the thermodynamic cell voltage of 1.23 V, appearing near +0.8 V in 0.01 M $HClO_4$ in Figure 1. Nonetheless, silver oxidation occurs near the voltage where oxygen reduction commences on platinum (+0.7 to +0.8 V). Thus, an opportunity exists whereby silver could serve as an effective, economical alternative to platinum if the overvoltage to oxygen reduction at silver could be lowered such that oxygen reduction commences near the silver oxidation potential.

To test the effectiveness in catalyzing oxygen reduction of BPA-covered preroughened silver, we prepared an experiment in which shuttered light (4 s off, 4 s on, 4 s off) was admitted to the surface in an oxygen-saturated solution. Photocurrent was observed at an applied potential significantly anodic of the voltage where oxygen reduction commences at silver in the dark (Figure 2). Continuous bubbling of oxygen largely removes the limitation of current by diffusion as evident from the near constant photocurrent level during the irradiation period. The height of the photocurrent response was found to be linearly dependent upon the laser power indicating a single photon excitation process. Observed oxygen reduction photocurrents (typically 6 μAmp per 0.15 cm^2 irradiated electrode area, or 0.04 mAmp/cm^2, with laser power of 100 mW at 5145 Å or a quantum yield of 0.000145) were recognized as comparable to those reported for photoelectrochemical reduction of aqueous

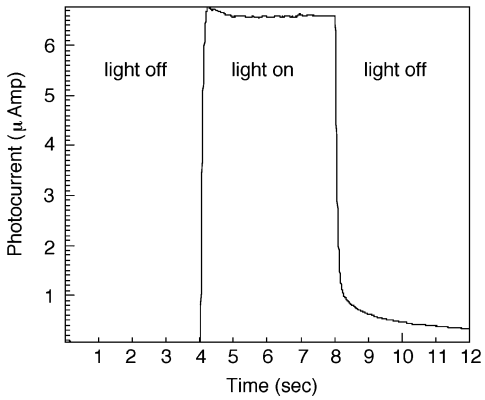

Figure 2. Photocurrent observed upon irradiation of a preroughened, BPA-covered silver electrode. Laser power, 100 mW, 5145 Å (Ar^+); solution, 0.1 M $NaClO_4$; pH 3.04; potential, +0.39 V vs RHE; oxygen gas bubbling continuously.

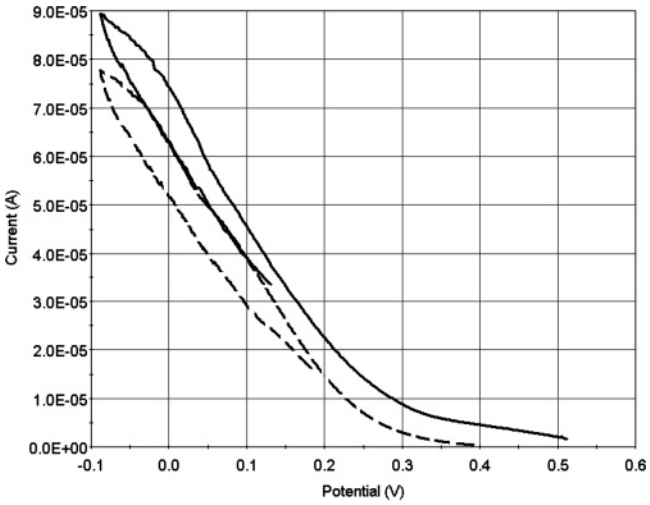

Figure 3. Cyclic voltammograms for BPA-covered silver during irradiation (—) and in the dark (---): Laser power. 100 mW, 5145 Å (Ar^+). Potentials are referenced to the RHE. Solution: 0.1 M $NaClO_4$, pH 3.04; scan rate, 10 mV/sec. The solution was saturated with oxygen by bubbling the gas through solution continuously.

carbon dioxide,[11,13,14] nitrite,[15] and nitrate[11,15] at similarly roughened silver after adjusting linearly for applied laser power, irradiated area, and reductant solution concentrations, for example, solubilities: $X_{CO_2}/X_{O_2} = (7.1 \times 10^{-4})/(2.5 \times 10^{-5}) = 28$ at 20 °C.

Comparison of the onset potential for oxygen reduction in the dark with that observed during irradiation is demonstrated in the cyclic voltammograms shown in Figure 3. The onset potential for oxygen reduction advances by nearly +200 mV at the irradiated electrode compared to that in the dark, revealing the photocatalytic utility of the method. To avoid surface reconstruction associated with silver oxidation, the applied voltages were held cathodic of the open circuit potential.

We associated the observed cathodic photocurrents with oxygen reduction by measuring the current response to shuttered light as a function of dissolved oxygen concentration. The solution was first saturated with dissolved oxygen by bubbling oxygen through the solution for 1 h. Then, the bubbling was ceased. Monitoring the oxygen content with a Hach dissolved oxygen meter we observed the oxygen content to drop from 330% air saturation (30.3 mg/L or 9.4×10^{-4} M), while the solution was agitated with bubbling, to a steady state of 235% air saturation (21.6 mg/L or 6.74×10^{-4} M) with the bubbling turned off. This is typical behavior for oxygen electrodes that

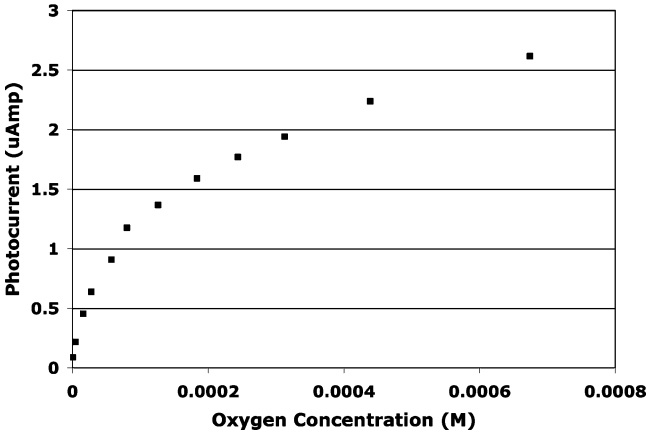

Figure 4. Photocurrent vs concentration of dissolved oxygen at a preroughened BPA-covered silver electrode. Laser power, 100 mW (5145 Å, Ar^+); solution, 0.1 M $NaClO_4$, pH 3.04; potential, +0.39 V referenced to RHE.

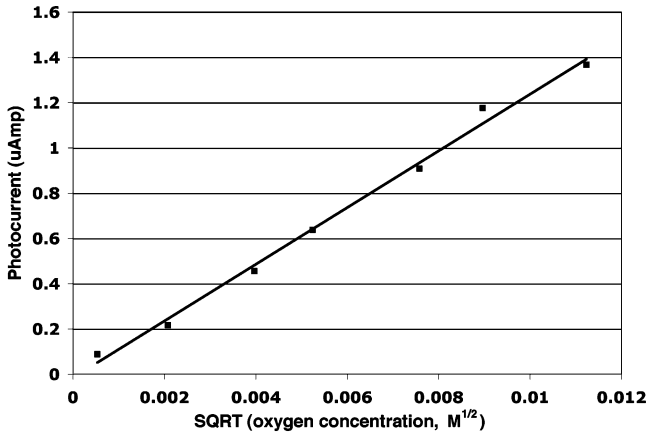

Figure 5. Photocurrent vs the square root of the dissolved oxygen concentration($\sqrt{[O_2]}$) at a preroughened BPA-covered silver electrode at low oxygen concentration. Laser power, 100 mW (5145 Å, Ar^+); potential, +0.39 V referenced to RHE.

depend upon diffusion of oxygen to the electrode, wherein diffusion is enhanced while the solution is agitated during bubbling. The shuttered photocurrent response was then measured. Purified nitrogen gas was then bubbled briefly through the solution to lower its oxygen content. After an attainment of a steady state without bubbling the photocurrent response was again measured. This process was repeated until the solution was oxygen free. The results are shown in Figure 4. The photocurrent signal drops to near zero with depletion of dissolved oxygen. Small residual photocurrents may be associated with scavenging of hydrated photoelectrons by protons and by the adsorbate.

Figure 5 plots the photocurrent measurements made at low oxygen concentration in Figure 4 versus the square root of the concentration. A linear relationship identifies the dependence of the rate of the photocatalyzed oxygen reduction reaction (the photocurrent) on $\sqrt{[O_2]}$. The square root dependence, as opposed to linear dependence, on oxygen concentration at low concentrations (below saturation) is characteristic[20] of a mechanism involving scavenging of hydrated photoelectrons. Similar square root dependence of the photocurrent on scavenger concentration has been observed for the reduction of nitrite at silver.[15]

We propose the following reaction scheme for the photocatalysis of oxygen reduction at a BPA-covered silver electrode:

$$Ag^0BPA + e- + h\nu \rightarrow Ag^0BPA^- \quad (1)$$

$$Ag^0BPA^- + O_2(aq) \rightarrow Ag^0BPA + O_2^-(aq) \quad (2)$$

where a metal-to-adsorbate charge transfer, or, alternatively, a surface-plasmon assisted photoemission from the silver electrode, yields a radical anion adsorbate. The radical anion (BPA^-) then serves as an electron source for delivery of a reducing equivalent to oxygen. With a small steady-state concentration of the BPA^- intermediate expected it is not surprising that the SERS of BPA adsorbed at roughened silver[21] does not readily provide spectroscopic evidence for the radical anion. The direct involvement of the BPA molecule in the transfer of electrons to oxygen is consistent however with the photochemistry observed for trans-4-stilbazole. There, photochemical attachment of atomic oxygen exclusively at the 4′-position of stilbazole[18] in the presence of dissolved oxygen implicated the direct role of the adsorbate in the reduction of diatomic oxygen. The first step in the electroreduction of oxygen, i.e., reduction of O_2 to O_2^- upon delivery of the first reducing equivalent, is the rate determining step.[22] Illumination of BPA-covered silver catalyzes this first step thereby reducing the overvoltage to oxygen reduction.

Testing the generality of the photoinduced delivery of reducing equivalents to available reductants in solution we examined oxygen-free solutions of iodine (I_2) and ferricyanide ($Fe[CN]_6^{3-}$). Electroreduction of these reductants, along with that of oxygen and BPA, is demonstrated in the cyclic voltammograms shown in Figure 6.

The associated shuttered admission of light to the preroughened, BPA-covered silver electrode in the presence of each of these dissolved reductant molecules is shown in Figure 7. Reduction of the solution bound reductants is demonstrated by photocurrent that is diffusion-limited during the central 4-second irradiation period. The rate of decay of the photocurrent increases inversely with the relative diffusion coefficients of the three reductants. Photoreductions of ferricyanide and iodine are reversed (oxidation current observed) when the light is turned off (from 8 to 12 s) while photoreduction of oxygen appears irreversible. For iodine, the reduction product is likely iodide ion (I^-) and the oxidation current observed subsequent to the irradiation period may be associated with oxidation of the silver electrode to silver iodide (AgI) in addition to, or instead of, the reoxidation of I^- to I_2.

While studying the photocatalyzed reduction of dissolved iodine at BPA-covered silver (discussed above) we observed photocurrent even when the preroughened silver electrode was *not* dipped in a BPA solution. Suspecting that, in this situation, iodine adsorbed from solution and then served to photocatalyze the reduction of other solution-bound iodine, we prepared to test the photocatalytic response of an iodine-coated silver electrode toward reduction of dissolved oxygen. A preroughened silver electrode was dipped for 5−10 min in a saturated aqueous solution of iodine (I_2). After rinsing in distilled water, the, now visibly brown, silver electrode was transferred to the 0.1 M $NaClO_4$ solution in the cell for photocurrent measurements. The results are shown in Figure 8.

Subsequent examination of the I_2-covered silver electrode with cyclic voltammetry (Figure 9) revealed the presence of AgI at the electrode surface. Formation of AgI during the dip results from the thermodynamically allowed coupling of silver oxidation and iodine reduction.

$$Ag(s) + {}^1/_2I_2(aq) \rightleftarrows AgI(s) \quad (3)$$

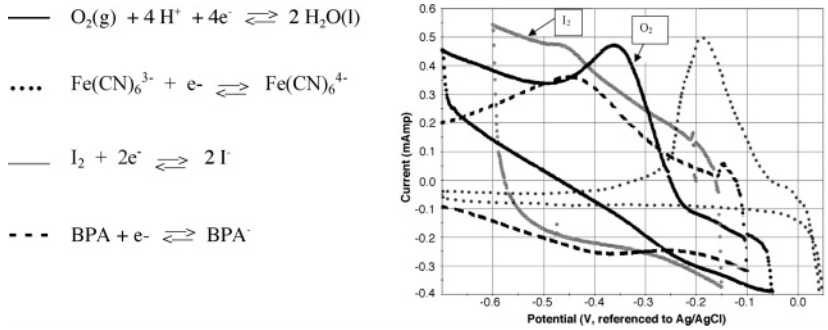

Figure 6. Cyclic voltammetry of other reducible molecules: oxygen (black line), potassium ferricyanide $K_3Fe(CN)_6$ (••••), iodine I_2 (gray line), and bis-1,2-(4-pyridyl)acetylene BPA (---); Ag/AgCl reference electrode.

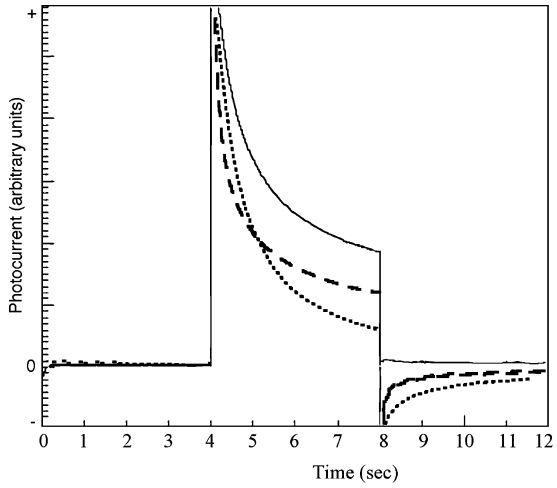

Figure 7. Photocurrent associated with reduction of oxygen (–, air saturated 0.1 M NaCl solution, diffusion coefficient 2.20×10^{-5} cm^2/sec), iodine (---, 5×10^{-4} M in 0.1 M NaCl, diffusion coefficient 1.37×10^{-5} cm^2/sec), and ferricyanide (•••, 1×10^{-3} M in 0.1 M NaCl, diffusion coefficient 0.718×10^{-5} cm^2/sec) during a 4 s off/4 s on/4 s off shuttered light experiment. Potential: −0.075 V referenced to Ag/AgCl).

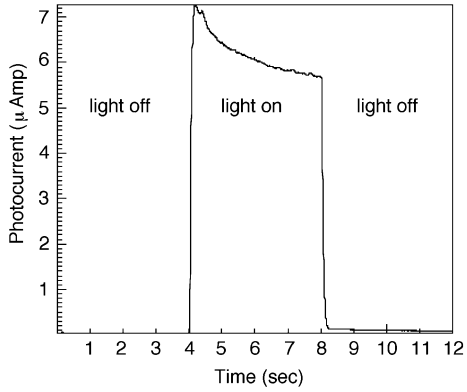

Figure 8. Photocurrent observed upon irradiation of a preroughened, I_2-covered silver electrode: laser power, 100 mW, 5145 Å (Ar^+); solution, 0.1 M $NaClO_4$, pH 3.04; potential, +0.37 V vs RHE; oxygen gas bubbling continuously.

Identical behavior was observed by Linnert et al.[16] for colloidal silver in the presence of either iodide ion or iodine. Reduction of AgI(s) appears as the first wave in the cathodic (negative) sweep of applied potential, followed by a wave accompanying reduction of dissolved oxygen. During the anodic return scan some reoxidation of silver to AgI(s) is observed, limited by availability of I^- from solution following diffusion away from the surface. Photocatalyzed reduction of dissolved oxygen was eliminated by electroreduction of the AgI(s) film. Using surface enhanced Raman scattering Sibbald et al.[23,24] characterize the

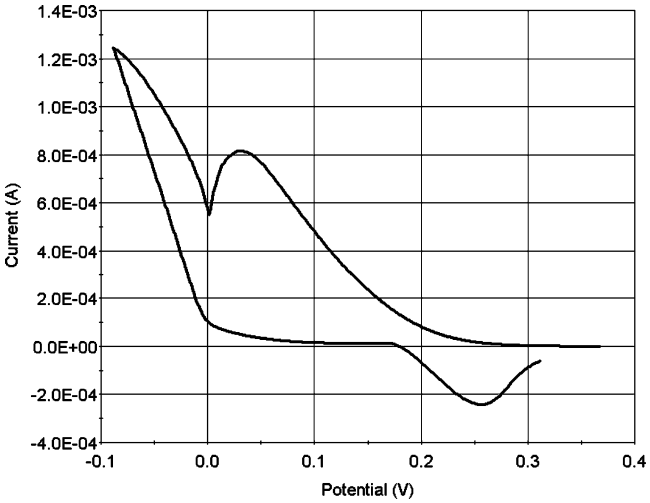

Figure 9. Cyclic voltammetry at I_2-covered silver electrode for an oxygen-saturated solution of 0.1 M $NaClO_4$, pH 3.04. Potentials referenced to the RHE. Scan rate is 20 mV/sec.

adsorption of I^- at silver as best represented as Ag_S-I, with Ag_S referring to the silver surface, and distinguishable in Raman stretching frequency from that in single-crystal AgI. In a detailed surface Raman study of iodide (I^-) adsorbed at a nanostructured silver surface[25] the spectra reveal surface species that are best described as "I_2-like" where proximal adsorbed I^- ions join. Thus, I_2 adsorbed at silver can be considered as another way to describe I^- at silver, that is, Ag_S-I_2 is equivalent to Ag_S-I.

With the recognition that the active adsorbate layer for iodine at silver was actually AgI (or, perhaps, Ag_S-I) we prepared a silver surface by anodizing a freshly polished silver electrode in a 0.1 M solution of potassium iodide passing 1 mC of anodic charge (5 mC per cm^2 electrode area). Instead of reversing the silver oxidation, as in a typical oxidation/reduction cycle used to roughen a silver electrode surface, the oxidation was stopped by taking the cell out of circuit. The AgI-coated silver electrode was then rinsed and moved to the 0.1 M $NaClO_4$ solution for photocurrent measurements. Thus the electrode was prepared *without* the usual preroughening or dipping in an adsorbate solution. The results are shown in Figure 10.

Not unexpectedly, the AgI-covered silver electrode shows effective photocatalysis of oxygen reduction equivalent to that for I_2-covered silver. The absence of photocurrent in the nitrogen-saturated solution, the steady-state photocurrent attained at long illumination times, and the increase in the photocurrent on moving from air- to O_2-saturated solutions preclude assignment of the response to illumination to photoreduction of the silver halide, a process well-known in photography. At the relatively anodic applied potentials, photoreduced AgI would be reoxidized such that no net photocurrent attributable to AgI

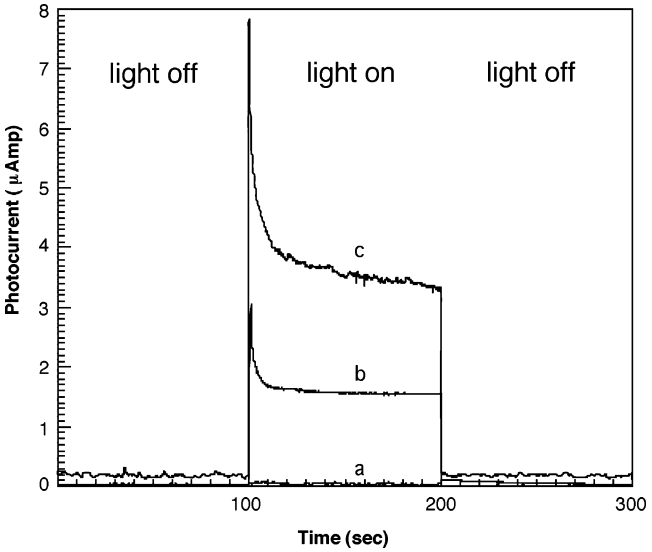

Figure 10. Photocurrent observed for an AgI-covered silver electrode for (a) nitrogen saturated solution (b), air saturated solution, and (c) oxygen saturated solution with oxygen bubbling continuously: laser power, 100 mW, 5145 Å (Ar^+); solution, 0.1 M $NaClO_4$, pH 3.04; potential, +0.35 V vs RHE. Elongated illumination time of 100 s.

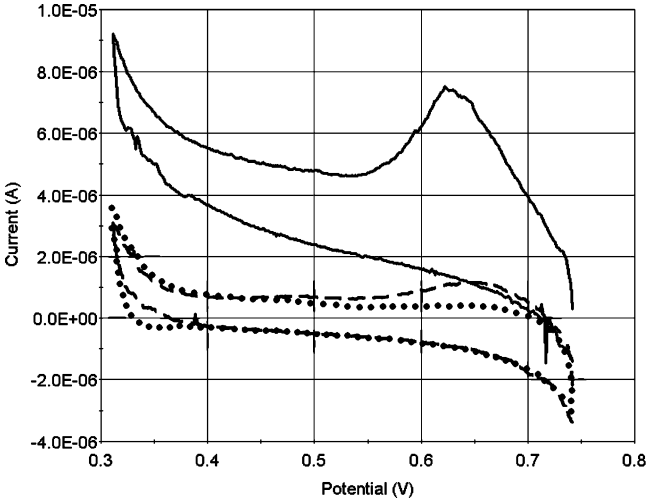

Figure 11. Cyclic voltammetry at AgI-covered silver electrode during irradiation (–) and in the dark (---) or an oxygen-saturated solution are compared with that for a nitrogen-saturated solution during irradiation (•••). Laser power, 100 mW, 5145 Å (Ar^+); solution, 0.1 M $NaClO_4$, pH 3.04; potential, +0.37 V vs RHE; oxygen or nitrogen gas bubbling continuously. Scan rate is 20 mV/sec.

reduction is realized. Nonetheless, the first step in the mechanism of transfer of electrons to oxygen likely involves photoreduction of Ag^+I^- to Ag^0I^- via electron transfer from the silver metal. The resultant zero oxidation silver is readily reoxidized back to Ag^+I^- by coupling with the reduction of oxygen diffusing to the surface. The process is then repeated in the attainment of steady-state photocurrent. The following reaction scheme is proposed for photocatalyzed reduction of oxygen at AgI-covered silver:

$$Ag^+I^- + e- + h\nu \rightarrow Ag^0I^- \quad (4)$$

$$Ag^0I^- + O_2(aq) \rightarrow Ag^+I^- + O_2^-(aq) \quad (5)$$

Recognizing the equivalence of adsorbed AgI to Ag_S-I_2, as discussed above, an alternate mechanism might be written

$$Ag_S-I_2 + e- + h\nu \rightarrow Ag_S-I_2^- \quad (6)$$

$$Ag_S-I_2^- + O_2(aq) \rightarrow Ag_S-I_2 + O_2^-(aq) \quad (7)$$

Again, analogous to the photocatalysis at BPA-covered silver, reduction of dissolved oxygen is catalyzed by delivery of the first reducing equivalent to oxygen in the rate determining step. Photosensitive iodide-covered silver colloids have been shown[23,24] to be capable of reducing a variety of solution-bound molecules, for example cytochrome *c*, whose reduction was found to be limited by the presence of dissolved oxygen that served to remove excess negative charge from the colloid.

In Figure 11 we probe the degree to which the oxygen overvoltage is lowered at AgI-covered silver upon illumination and compare to the onset voltage for oxygen reduction in the dark. Oxygen (and AgI) commence reduction near +0.35 V in the dark. Upon illumination, we observe oxygen reduction at potentials nearly 400 mV anodic of where oxygen reduces in the dark. The anodic range is limited only by the oxidation of silver in perchlorate (onset voltage near +0.74 V vs RHE), that is, at voltages comparable to the onset voltage for oxygen reduction at platinum. That the photocurrent is associated with oxygen reduction is assured by the subsequent study in nitrogen-saturated (oxygen-free) electrolyte during illumination and its ready comparison with the cyclic voltammogram recorded in the dark.

To this point we have reported photocurrents excited with 5145 Å (Ar^+) laser excitation. To better understand the electronic transitions responsible for delivering electrons to oxygen, we now examine the wavelength dependence of the photocurrent, referred to as the "action" spectrum. An extinction spectrum is needed for comparison; however, unlike stabilized colloidal suspensions of silver that permit convenient gathering of the percent transmission of solution,[26,27] the extinction spectrum for the bulk silver electrode must be determined from reflectance measurements. Toward this purpose we constructed a sequence of mirrors to redirect the source of a Cary 219 UV–vis spectrophotometer to and from the silver electrode surface. Surface sensitivity of the reflectance measurements was realized by modulating the applied potential at the electrode and tracking the spectrophotometric response.[28] The sensitivity of the Cary 219 was sufficient that signal response could be recorded without the need for a lock-in amplifier. The electrode potential was modulated sinusoidally by ±0.3 V about a central bias voltage of −0.4, −0.5, or −0.6 V (vs Ag/AgCl) at a frequency of 0.1 Hz. Because both BPA and iodine reduce within this modulating voltage range of −0.1 to −0.9 V (cf. Figure 6) the preroughened silver electrode was instead dipped in a solution saturated in trans-1,2-bis(4-pyridyl)ethylene (BPE). BPE, which is the double-bonded equivalent to BPA, does not reduce before −1.2 V (vs Ag/AgCl), that is, outside the modulation range, yet offers a similar metal binding site and absorption spectrum (λ_{max} = 330 nm) to that of BPA. The component of the spectrophotometric response that was in-phase with the modulation was extracted by Fourier analysis and recorded every 5 nm from 350 to 800 nm. The results are shown in Figure 12 along with examples of the voltage modulation and its spectrophotometric response at select wavelengths for the −0.5 V bias.

The modulated electroreflectance spectrum of BPE-covered silver reveals two derivative shapes, representing extinction maxima, centered just below 400 and just above 500 nm and suggests another resonance on approaching the near-infrared. The absorbance near 400 nm is readily recognized as the surface plasmon resonance. The absorbance above 500 nm is less easily

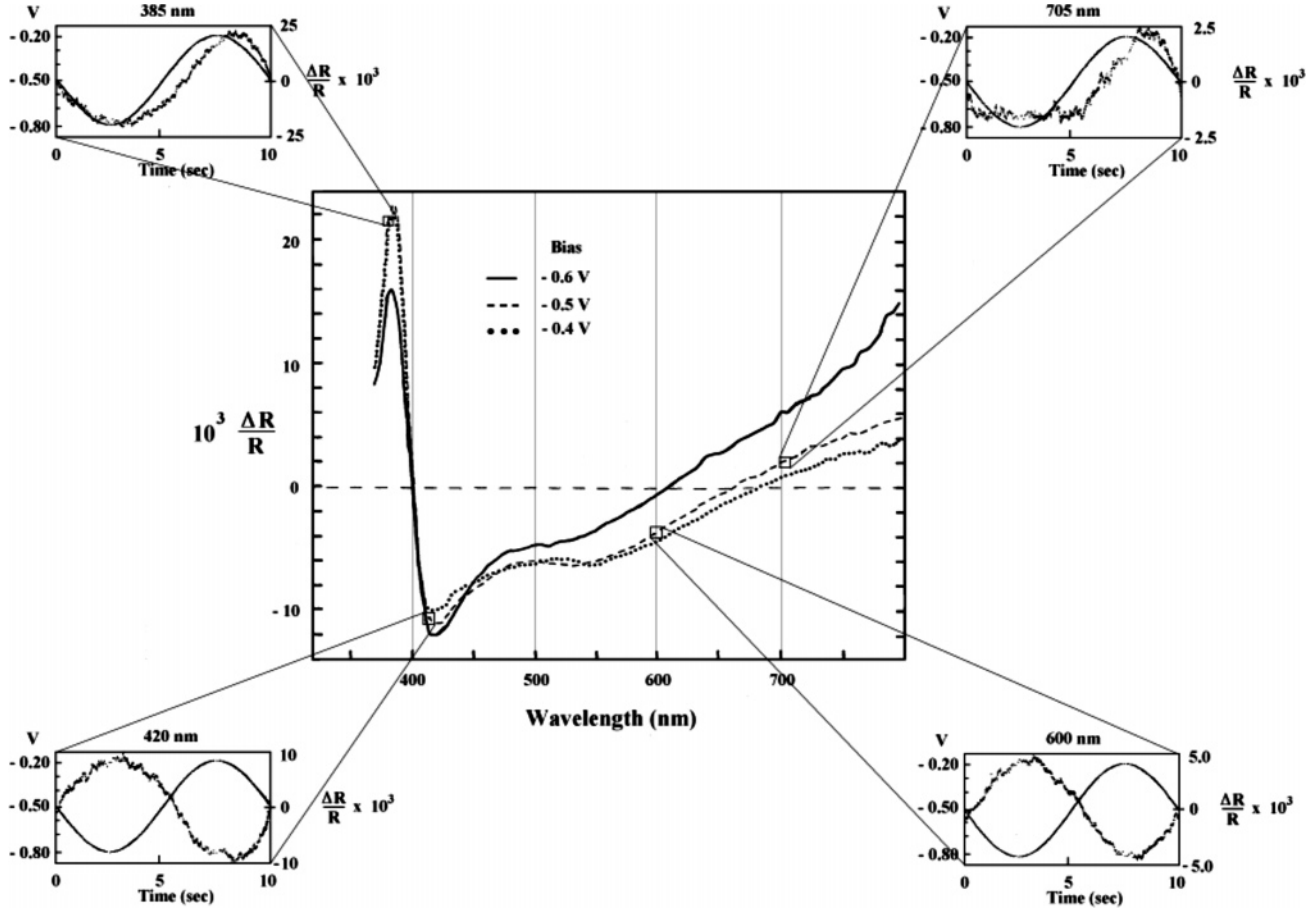

Figure 12. Modulated electroreflectance spectrum of BPE-covered silver. Bias voltages: −0.4 (•••), −0.5 (---), and −0.6 V (–) vs Ag/AgCl reference. Frequency 0.1 Hz. Signal averaged for 10 cycles at each wavelength before changing wavelength. Insets show the sinusoidal voltage modulation (smooth curve) and the accompanying normalized reflectivity changes ($\Delta R/R$) at select wavelengths within the spectrum recorded at bias −0.5 V.

defined and supports a smaller extinction than, and is dragged below zero $\Delta R/R$ by overlap with the long wavelength tail of, the surface plasmon resonance. While the surface plasmon resonance does not appear to shift much with bias voltage the feature above 500 nm and the near-infrared feature do show some bias dependence. The large red or near-infrared resonance appears to shift to shorter wavelengths with more negative bias. This behavior suggests an adsorbate-to-metal charge transfer assignment for the red or near-infrared absorbance where the resonant photon shifts to bluer wavelengths when a lower metal work function (Φ[V]) accompanies a move to more negative bias, that is, hc/λ = I.E.(ad) − Φ[V]. Conversely, bias dependence in the electroreflectance near 425 nm appears to suggest that the resonance just above 500 nm shifts to the red with increasingly negative bias, characteristic of a complementary metal-to-adsorbate charge-transfer excitation.

The "action" spectra for BPA-covered silver and I_2-covered silver are compared with the electroreflectance of BPE-covered silver in Figure 13. Maxima in the observed photocurrents, for both the BPA- and I_2-covered electrodes, appear near 400 nm and between 500 and 600 nm. The action spectra are remarkably similar for the two very different adsorbates, suggesting that the metal surface is primarily responsible for the wavelength dependence of the photocurrent and supporting our contention that the electroreflectance spectrum of BPE-covered silver serves as an approximate extinction spectrum for the system. The 400 nm peak in the action spectrum of both adsorbates reveals the effectiveness of the silver surface plasmon in coupling to photoemission of electrons that are subsequently scavenged by dissolved oxygen. Surface roughening[12] allows some of the hot electrons excited by decay of the surface plasmon to satisfy the conservation of momentum constraint and travel along the surface normal ejecting into solution. Similar correspondence between photocurrent maxima and surface plasmon resonance has been reported for photocurrents that accompany the scavenging of photoelectrons by carbon dioxide[12,13] and nitrite.[15]

Even more interesting is the apparent resonance between the photocurrent for oxygen reduction and the weak extinction feature in the electroreflectance spectrum between 500 and 600 nm. Oxygen reduction photocurrents equivalent to, or exceeding those observed in resonance with the surface plasmon at 400 nm are observed in this region of the "action" spectrum despite its weak extinction in the electroreflectance. Broadening of the surface plasmon resonance upon surface roughening is cited[12] as the source of photocurrents accompanying CO_2 scavenging observed with wavelengths in 500−600 nm region. However, our observations of disproportionately large oxygen reduction photocurrent within this region of weak electroreflectance extinction, compared to photocurrents observed near the intense surface plasmon absorption at 400 nm, may suggest a distinctly more effective mechanism of photoemission excitation with wavelengths between 500 and 600 nm. Because its propagation vector is parallel to the surface normal a metal-to-adsorbate charge transfer may be expected to be intrinsically more effective at delivering electrons to available reductants than that fraction of hot electrons from a decaying surface plasmon that happen to also run parallel to the surface normal. The situation is not unlike that observed for SERS excitation profiles for

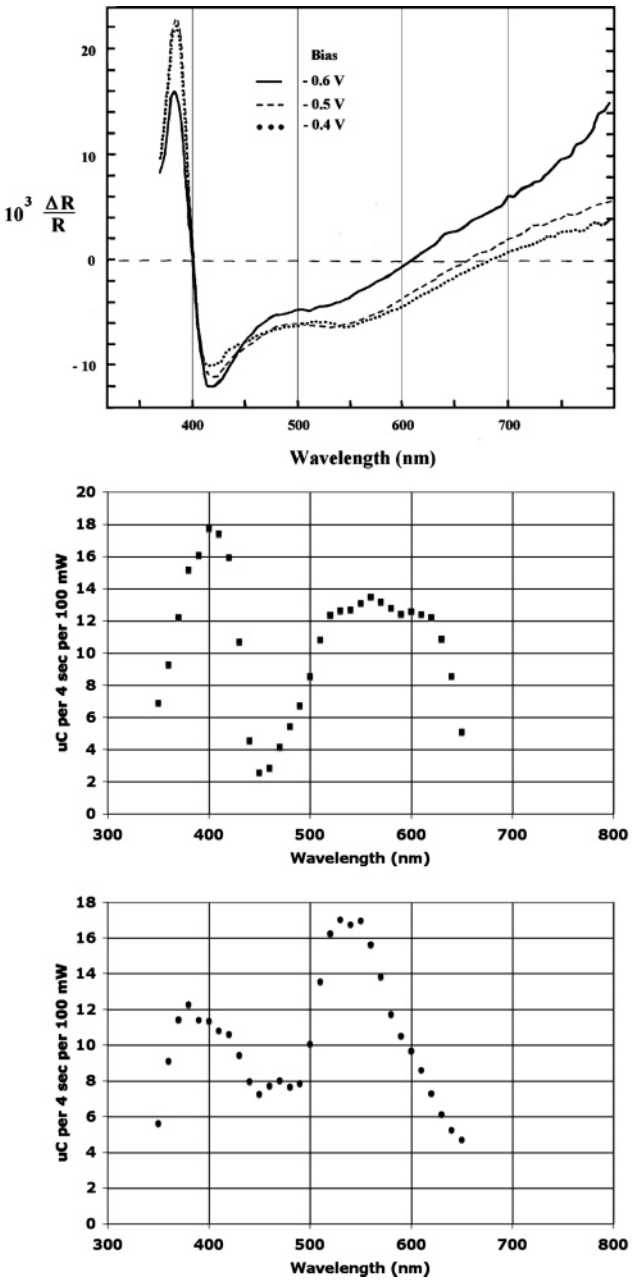

Figure 13. Modulated electroreflectance spectrum of BPE-covered silver (top); "action" spectrum (μC charge passed during a 4-second illumination period) for I_2-covered silver (middle) at +0.416 V vs RHE; "Aaction" spectrum for BPA-covered silver (bottom) at +0.361 V vs RHE; 300 W xenon light source passed through a monochromator (resolution 20 nm fwhm) and normalized to equal incident light intensity of 100 milliwatt. All solutions are air saturated.

adsorbates at silver colloids in the same (500−600 nm) region. Both von Raben et al.[29] and Feilchenfeld et al.[30] report large surface Raman intensities using excitation wavelengths in resonance with relatively weak longer wavelength features in the extinction spectra of silver colloids. In both studies, the longer wavelength extinctions are assigned to surface plasmon resonances at aggregated colloids in agreement with computations simulating nonspherical aggregates by Kerker et al.[31] Still troubling is why a lower extinction surface plasmon resonance from aggregated roughness features should yield equal or stronger photocurrents than the large extinction surface plasmon resonance at 400 nm. This observation combined with the dependence of the electroreflectance spectrum near 425 nm on bias potential serve to retain metal-to-adsorbate charge transfer as a viable first step for photocatalysis in the 500−600 nm wavelength region.

In summary, we present evidence of photocatalyzed reduction of dissolved oxygen at adsorbate-covered silver electrodes. The photocatalysis permits oxygen reduction to proceed at voltages approaching the oxidation potential of silver in a perchlorate medium and rivaling the onset potential for oxygen reduction at platinum. Our studies of BPA and I_2 (or AgI) adsorbates suggest applicability of a broad range of adsorbates, perhaps limited to those that are reducible but not appreciably oxidizable. With silver selling for 1/100th the price of platinum, adsorbate-covered silver may offer an economical alternative to platinum loading at fuel cell cathodes. The modest photocurrents that we report for oxygen reduction at silver may be extrapolated to a level practical to fuel cells when it is realized that the economics of silver allow for the entire cathode to be constructed of high surface area porous silver, as opposed to finely dispersed platinum on carbon. Sterlitech Corporation of Kent, WA, for example, offers silver membrane "filters" of a variety of average pore sizes. If we used the 0.8 μ pore size, 0.05 mm thick Sterlitech silver membrane for the cathode, which provides an effective surface area of 146 cm^2 per cm^2 of apparent area (πr^2) and an average pore size large enough to propagate light of visible and near UV wavelengths, then, scaling our reported photocurrent density of 0.04 mAmp/cm^2 to the effective area, we can realize current densities of 5.84 mAmp/cm^2. In a recent U.S. Department of Energy (DOE) Funding Opportunity Announcement entitled "Research and Development of Fuel Cell Technology for the Hydrogen Economy" (Announcement DE-PS36-06GO96017) DOE established the 2010 technical target for the specific activity of fuel cell electrocatalysts (Table 2 in the DOE Announcement) at 0.720 mAmp/cm^2. These calculations suggest the realistic application of a silver cathode in fuel cells. As with SERS, the nature of the excitation mechanism is difficult to nail down, but our wavelength-dependence studies point to successful photocatalysis at visible and near-ultraviolet wavelengths. Further experimentation directed toward determination of the optimal AgI film thickness for photocatalysis and actual construction of a fuel cell with a silver cathode that is accessible to a radiation source are in progress. Unlike silver, gold is not limited by its oxidation potential, which lies above the 1.23 V thermodynamic voltage of a fuel cell. Additionally, we are exploring the applicability of gold cathodes to photocatalysis of the oxygen reduction reaction encouraged by SERS experiments at roughened gold. While not enjoying the extreme economic advantage that silver enjoys gold would not be limited by its oxidation potential, like silver is, and holds significant promise for lowering the oxygen overvoltage *below*, not just equivalent to, that on platinum.

Acknowledgment. We gratefully acknowledge partial support for this research effort from the Faculty Research Grant Program administered by the Office of Research at Fordham University.

References and Notes

(1) Tarasevich, M. R.; Sadkowski, A.; Yeager, E. in *Comprehensive Treatise of Electrochemistry*: *Kinetics and Mechanism of Electrode Processes*; Conway, B. E., Bockris, J. O., Yeager, E., Khan, S. U. M., Eds.; Plenum Press: New York 1983; Vol. 7, p 301.

(2) Gottesfeld, S.; Zawodzinski, T. A. in *Advances in Electrochemical Science and Engineering*; Alkire, R. C., Kolb, D. M., Eds.; Wiley-VCH: Weinham, Germany, 1997; Vol. 5, 195.

(3) Markovic, N. M.; Schmidt, T. J.; Stamenkovic, V.; Ross, P. N. *Fuel Cells* **2001**, *1*, 105.

(4) Tamura, K.; Ocko, B. M.; Wang, J. X.; Adzic, R. R. *J. Phys. Chem. B* **2002**, *106*, 3896.
(5) Mano, N.; Fernandez, J. L.; Kim, Y.; Shin, W.; Bard, A. J.; Heller, A. *J. Am. Chem. Soc.* **2003**, *125*, 15290.
(6) Zhang, J.; Mo, Y.; Vukmirovic, M. B.; Klie, R.; Sasaki, K.; Adzic, R. R. *J. Phys. Chem. B* **2004**, *108*, 10955.
(7) Shao, M. H.; Adzic, R. R. *J. Phys. Chem. B* **2005**, *109*, 16563.
(8) Zhang, J.; Lima, F. H. B.; Shao, M. H.; Sasaki, K.; Wang, J. X.; Hanson, J.; Adzic, R. R. *J. Phys. Chem. B* **2005**, *109*, 22701.
(9) Henglein, A. *J. Phys. Chem.* **1993**, *97*, 5457.
(10) Sass, J. K.; Sen, R. K.; Meyer, E.; Gerisher, H. *Surf. Sci.* **1974**, *44*, 515.
(11) Kostecki, R.; Augustynski, J. *J. Appl. Electrochem.* **1993**, *23*, 567.
(12) Kostecki, R.; Augustynski, J. *J. Appl. Phys.* **1995**, *77*, 4701.
(13) Fedurco, M.; Shklover, V.; Augustynski, J. *J. Phys. Chem B* **1997**, *101*, 5158.
(14) Zheng, J.; Lu, T.; Cotton, T. M.; Chumanov, G. *J. Electroanal. Chem.* **2002**, *518*, 6.
(15) Zheng, J.; Lu, T.; Cotton, T. M.; Chumanov, G. *J. Phys. Chem B* **1999**, *103*, 6567.
(16) Linnert, T.; Mulvaney, P.; Henglein, A. *J. Phys. Chem.* **1993**, *97*, 679.
(17) Chance, R. R.; Prock, A.; Silbey, R. *Adv. Chem. Phys.* **1978**, *37*, 1.
(18) McMahon, J. J. Gergel, T. J.; Otterson, D. M.; McMahon, C. A.; Kabbani, R. M. *Surf. Sci.* **1999**, *440*, 357.
(19) Tanner, M., Ph.D. Thesis, Universitat Vern, 1980.
(20) Brodsky, A. M.; Gurevich, Y. Y. *Sov. Phys. JETP* **1968**, *54*, 213.
(21) McMahon, J. J.; Breen, K.; Barry, M. S. *Proc. Int. Conf. Raman Spectrosc., 20th* **2006**, 181.
(22) Sepa, D. B.; Vojnovic, M. V.; Damjanovic, A. *Electrochim. Acta* **1981**, *26*, 781.
(23) Sibbald, M. S.; Chumanov, G.; Cotton, T. M. *J. Phys. Chem.* **1996**, *100*, 4672.
(24) Sibbald, M. S.; Chumanov, G.; Cotton, T. M. *J. Electroanal. Chem.* **1997**, *438*, 179.
(25) Chumanov, G.; Sibbald, M. S.; Cotton, T. M. *J. Phys. Chem. B* **1998**, *102*, 10836.
(26) Creighton, J. A.; Blatchford, C. E.; Albrecht, M. G. *J. Chem Soc. Faraday Trans.* **1979**, *2*, 75.
(27) Kerker, M.; Siiman, O.; Bumm, L. A.; Wang, D.-S. *Appl. Opt.* **1980**, *19*, 3253.
(28) Kolb, D. M. *J. Physique* **1983**, *44*, 137.
(29) von Raben, K. U.; Chang, R. K.; Laube, B. L.; Barber, P. W. *J. Phys. Chem.* **1984**, *88*, 5290.
(30) Feilchenfeld, H.; Siiman, O. *J. Phys. Chem.* **1986**, *90*, 2163.
(31) Kerker, M.; Siiman, O.; Wang, D.-S. *J. Phys. Chem.* **1984**, *88*, 3168.